Jet production at HERA*

C. Glasman†
(on behalf of the ZEUS and H1 Collaborations)
Universidad Autónoma de Madrid, Spain

Abstract

Recent results from jet production in deep inelastic ep scattering to investigate parton dynamics at low x are reviewed. The results on jet production in deep inelastic scattering and photoproduction used to test perturbative QCD are discussed and the values of $\alpha_s(M_Z)$ extracted from a QCD analysis of the data are presented.

1 Introduction

Jet production in neutral-current (NC) deep inelastic ep scattering (DIS) and photoproduction provide tests of perturbative QCD (pQCD) calculations and of the parametrisations of the parton distribution functions (PDFs) in the proton. Jet cross sections allow the determination of the fundamental parameter of QCD, the strong coupling constant α_s, and help to constrain the proton PDFs.

Up to leading order (LO) in α_s, jet production in NC DIS proceeds via the quark-parton model (QPM) ($Vq \to q$, where $V = \gamma^*$ or Z^0, Fig. 1a), boson-gluon fusion (BGF) ($Vg \to q\bar{q}$, Fig. 1b) and QCD-Compton (QCDC) ($Vq \to qg$, Fig. 1c) processes. The jet production cross section is given in pQCD by the convolution of the proton PDFs and the subprocess cross section,

$$d\sigma_{\text{jet}} = \sum_{a=q,\bar{q},g} \int dx \; f_a(x, \mu_{F_p}) \; d\hat{\sigma}_a(x, \alpha_s(\mu_R), \mu_R, \mu_{F_p}),$$

where x is the fraction of the proton's momentum taken by the interacting parton, f_a are the proton PDFs, μ_{F_p} is the proton factorisation scale, $\hat{\sigma}_a$ is the subprocess cross section and μ_R is the renormalisation scale.

The main source of jets at HERA is hard scattering in photon-proton (photoproduction) interactions in which a quasi-real photon ($Q^2 \approx 0$, where Q^2 is the virtuality of the photon) emitted by the electron beam interacts with a parton from the proton to produce two jets in the final state. In LO QCD, there are two processes which contribute to the jet photoproduction cross section: the resolved process (Fig. 1d), in which the photon interacts through its partonic content, and the direct process (Fig. 1e), in which the photon interacts as a point-like particle.

*Talk given at the "XXXIV International Symposium on Multiparticle Dynamics", Sonoma County, California, USA, July 26$^{\text{th}}$ - August 1$^{\text{st}}$, 2004.

†Ramón y Cajal Fellow.

The cross section for the process $ep \to e$ + jet + jet + X is given by the convolution of the flux of photons in the electron, the parton densities in the proton, the parton densities in the photon and the subprocess cross section:

$$d\sigma_{ep\to\text{jet jet}} = \sum_{i,j} \int_0^1 dy\, f_{\gamma/e}(y) \int_0^1 dx_\gamma\, f_{i/\gamma}(x_\gamma, \mu_{F_\gamma}) \int_0^1 dx_p\, f_{j/p}(x_p, \mu_{F_p})\, d\hat{\sigma}_{i(\gamma)j}(i(\gamma)j \to \text{jet jet}),$$

where $f_{\gamma/e}$ is the flux of photons in the electron, usually estimated using the Weizsäcker-Williams approximation, y is the inelasticity variable, $f_{j/p}$ are the parton densities in the proton, determined from global fits, x_p is the proton momentum taken by the interacting parton, μ_{F_p} is the proton factorisation scale, $f_{i/\gamma}$ are parton densities in the photon, determined from fits to deep inelastic $e\gamma$ data, x_γ is the photon momentum taken by the interacting parton, μ_{F_γ} is the photon factorisation scale, and $d\hat{\sigma}_{i(\gamma)j}(i(\gamma)j \to \text{jet jet})$ is the subprocess cross section, which is calculable in pQCD at any order.

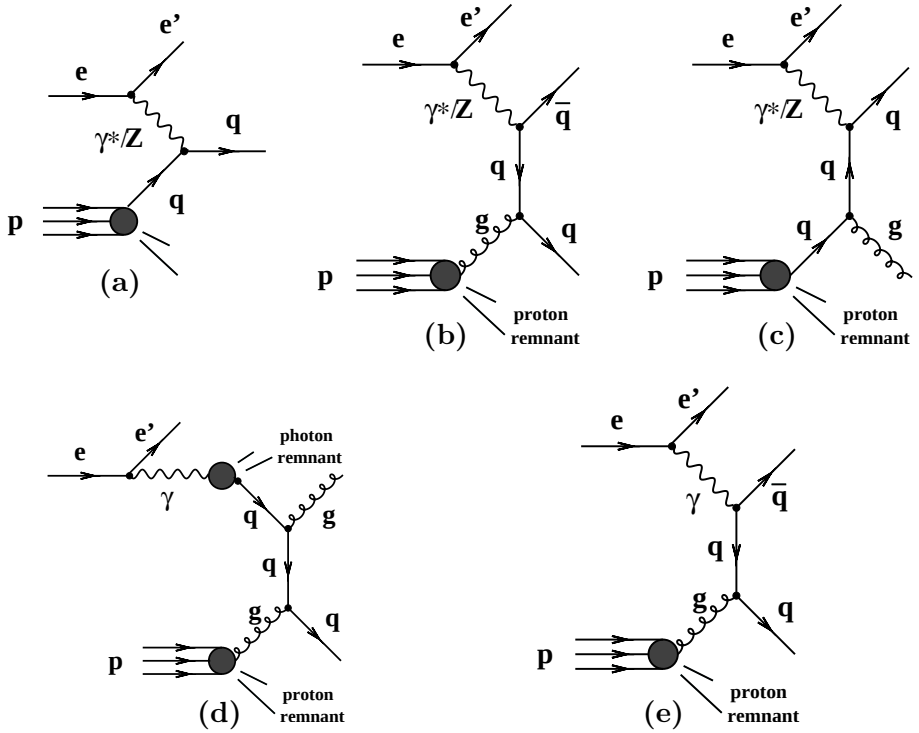

Figure 1: Examples of Feynman diagrams for deep inelastic ep scattering processes: (a) quark-parton model, (b) boson-gluon fusion and (c) QCD Compton. Examples for photoproduction processes: (d) resolved and (e) direct.

All the data accumulated from HERA [1, 2] and fixed-target [3] experiments have allowed a good determination of the proton PDFs over a large phase space and the evolution of the PDFs with the scale μ_{F_p} for large scales has been successfully described by the DGLAP evolution equations [4]. Measurements of jet production in NC DIS [5, 6] and photoproduction [7, 8] have provided accurate tests of pQCD and a determination of the fundamental parameter of the theory, α_s. Most of these measurements refer to the production of jets irrespective of their partonic origin –quarks or gluons– and, therefore, have provided general tests of the partonic

structure of the short-distance process and of combinations of the proton and/or photon PDFs. The identification of quark- and gluon-initiated jets would allow more stringent tests of the QCD predictions.

At high scales, calculations using the DGLAP evolution equations have been found to give a good description of the data up to next-to-leading order (NLO). Therefore, by fitting the data with these calculations, it has been possible to extract accurate values of α_s and the gluon density of the proton. However, for scales of $E_T^{\rm jet} \sim Q$, where $E_T^{\rm jet}$ is the jet transverse energy, large values of the jet pseudorapidity, $\eta^{\rm jet}$, and low values of x discrepancies between the data and the NLO calculations have been observed. This could indicate a breakdown of the DGLAP evolution and the onset of BFKL [9] effects. These discrepancies could also be explained by assigning a partonic structure to the exchanged virtual photon or a large contribution of higher-order effects at low Q^2.

This report includes recent results of the studies on parton evolution at low x from the H1 Collaboration, namely forward-jet cross sections as a function of x and the azimuthal correlation between the hard jets in dijet events in NC DIS, and the tests of pQCD at high scales from the ZEUS Collaboration, namely dijet and three-jet cross sections in NC DIS, measurements of the internal structure of jets in photoproduction and NC DIS and the study of the substructure dependence of jet cross sections in photoproduction.

2 Parton evolution at low Bjorken-x

To leading logarithm accuracy, the DGLAP evolution is equivalent to the exchange of a parton cascade with the exchanged partons strongly ordered in virtuality (Fig. 2). The DGLAP equations sum the leading powers of $\alpha_s \log Q^2$ in the region of strongly-ordered transverse momenta. However, DGLAP evolution is expected to breakdown at low x since only leading logarithms in Q^2 are resummed and contributions from $\log 1/x$ are neglected. These terms need to be taken into account since when $\log Q^2 \ll \log 1/x$, terms proportional to $\alpha_s \log 1/x$ become important.

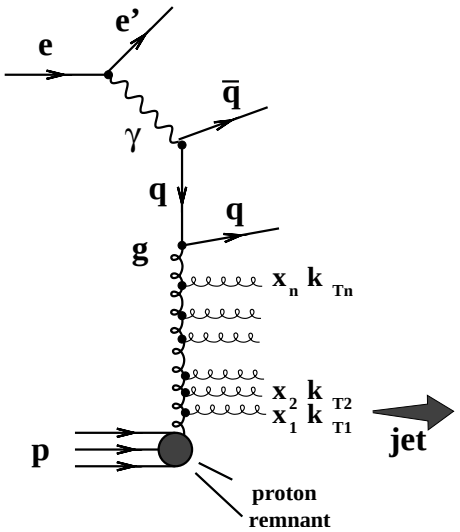

Figure 2: Example of Feynman diagram for forward jet production in NC DIS at low x.

Several theoretical approaches exist which account for low-x effects not incorporated into the

DGLAP evolution. They are: (i) the BFKL evolution which resums large $\log(1/x)$ terms to all orders, this approach works at very low x and presents no k_T ordering, the integration is taken over the full k_T phase scape of the gluons and the calculations make use of off-shell matrix elements together with unintegrated PDFs; (ii) the CCFM [10] evolution provides angular-ordered parton emission and works for low and larger x, it is equivalent to BFKL for $x \to 0$ and to DGLAP at large x; (iii) the virtual-photon structure mimicks higher-order QCD effects at low x by introducing a second k_T-ordered parton cascade on the photon side [11] à la DGLAP, the resolved contribution is expected to contribute for $(E_T^{\rm jet})^2 > Q^2$ and suppressed with increasing Q^2.

There exist several programs to calculate pQCD predictions of jet cross sections in NC DIS, eg DISENT [12] and NLOJET [13]. These programs use the DGLAP evolution equations. Higher-order effects can be mimicked by the parton-shower approach in leading-logarithm Monte Carlo models like RAPGAP [14], which includes direct or direct plus resolved processes in virtual-photon interactions. Low-x effects not included in the DGLAP evolution are incorporated in Monte Carlo models like CASCADE [15] and ARIADNE [16]. CASCADE is based on the k_T-factorised unintegrated parton distributions and follows the CCFM evolution, whereas ARIADNE generates non-k_T ordered parton cascades based on the color dipole model (CDM).

Experimentally, deviations from the DGLAP evolution can be expected at low x and forward-jet rapidity since parton emission along the exchanged gluon ladder (see Fig. 2) increases with decreasing x. Another method to obtain evidence for DGLAP breakdown is to study the azimuthal correlation between the two hardest jets. In DGLAP, partons entering the hard process with negligible k_T produce a back-to-back configuration at LO. Values of $\Delta\phi < 180^\circ$ occur in DGLAP due to higher-order QCD effects. In models which predict a significant proportion of partons entering the hard process with large k_T, the number of events with small $\Delta\phi$ will increase.

2.1 x dependence of the forward-jet cross section

The forward-jet cross section has been measured [17] for jets identified with the k_T cluster algorithm in the longitudinally inclusive mode in the laboratory frame. Events with at least one jet of transverse energy $E_{T,\rm LAB}^{\rm jet} > 3.5$ GeV and $1.7 < \eta_{\rm LAB}^{\rm jet} < 2.8$ were selected. The events are required to fulfill the additional conditions: (i) $x_{\rm jet} = E_{\rm jet}/E_p > 0.035$, where E_p is the proton-beam energy, and (ii) $0.5 < (E_T^{\rm jet})^2/Q^2 < 5$, following the proposal of Mueller and Navelet [18] such as to allow for a large-level arm of evolution in x and to restrict the evolution in Q^2. The measurements were made in the kinematic region given by $5 < Q^2 < 85$ GeV^2 and $0.0001 < x < 0.004$.

Figure 3 shows the forward-jet cross section as a function of x. The measured cross section rises with decreasing x. The NLO calculation corrected for hadronisation effects obtained using the program DISENT with the renormalisation scale $\mu_R^2 = 45$ GeV^2, the average $(E_T^{\rm jet})^2$ of the data, and the CTEQ6 parametrisations of the proton PDFs, is compared to the data in Fig. 3a. The measured cross section is well described by the prediction for large values of x, but at low x values there is a large excess of data with respect to the calculation. This prediction is based on DGLAP evolution and so it is not expected to work in this region of phase space.

Figure 3b shows the comparison with the predictions of different leading-logarithm parton-shower Monte Carlo models. The prediction of RAPGAP including only direct processes is similar to the NLO calculation. Once the contribution from resolved processes is included, a

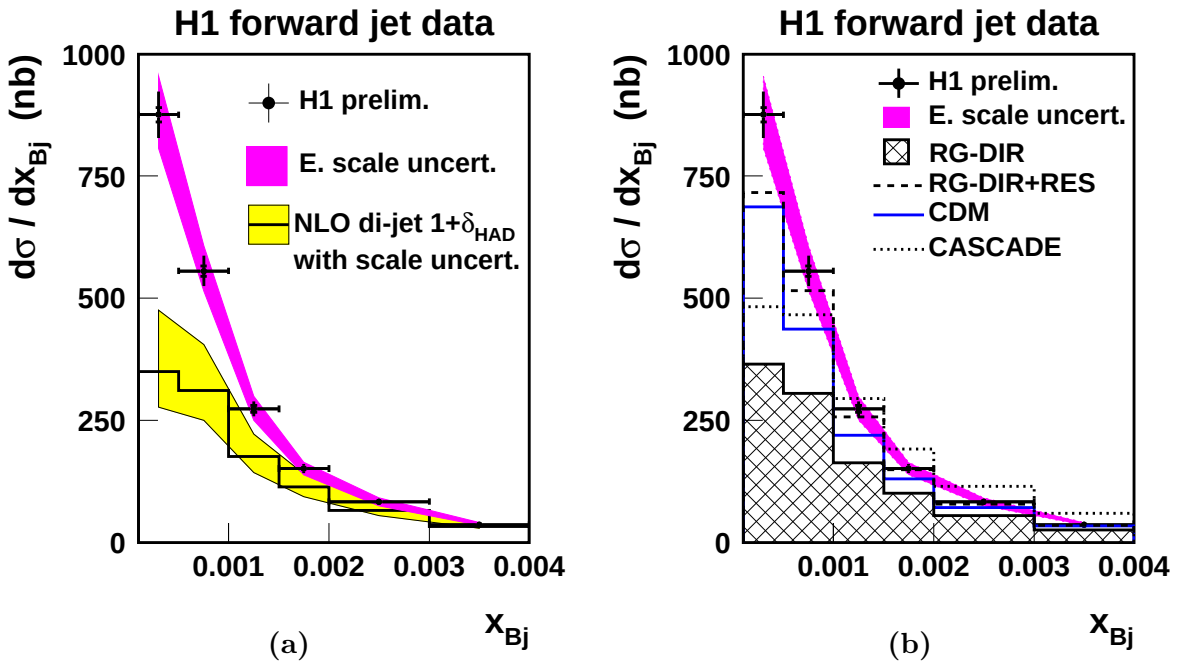

Figure 3: Measured forward-jet cross section (dots) [17] as a function of Bjorken x. For comparison, the predictions of (a) DISENT and (b) RAPGAP (RG), ARIADNE (CDM) and CASCADE are also included.

better description of the data is obtained for x down to 0.001. The CASCADE prediction, based on the CCFM evolution, does not reproduce the shape of the data, whereas the prediction from CDM describes the data for $x > 0.0015$. In conclusion, no model can describe the sharp rise of the data at very low x, which remains a challenge and demands improved approximations to QCD in that region of phase space.

2.2 Azimuthal jet separation

The azimuthal correlation between the two hard jets in dijet events has been measured [19] using the k_T-cluster algorithm in the longitudinally inclusive mode in the $\gamma^* p$ centre-of-mass frame. The measurements were made in the kinematic region given by $5 < Q^2 < 100$ GeV^2 and $10^{-4} < x < 10^{-2}$. The cross sections refer to jets of $E_T^* > 5$ GeV, $-1 < \eta^{\rm jet}_{\rm LAB} < 2.5$ and $E^*_{T,\rm max} > 7$ GeV, where E_T^* is the jet transverse energy in the $\gamma^* p$ centre-of-mass frame. Figure 4a shows the measured distribution as a function of the azimuthal separation in different Q^2 regions. A significant fraction of events is observed at small azimuthal separations. Since a measurement of a multi-differential cross section as a function of x, Q^2 and $\Delta\phi^*$ would be very difficult due to large migrations, the fraction of the number of dijet events with an azimuthal separation between 0 and α, where α was taken as $\alpha = \frac{2}{3}\pi$, was measured instead. The fraction S, defined as

$$S = \frac{\int_0^\alpha N_{\rm 2jet}(\Delta\phi^*, x, Q^2) d\Delta\phi^*}{\int_0^\pi N_{\rm 2jet}(\Delta\phi^*, x, Q^2) d\Delta\phi^*},$$

is better suited to test small-x effects than a triple-differential cross section.

The measured fraction S as a function of x in different regions of Q^2 is presented in Fig. 4b. The data rise towards low x values, especially at low Q^2. The predictions from DISENT, which

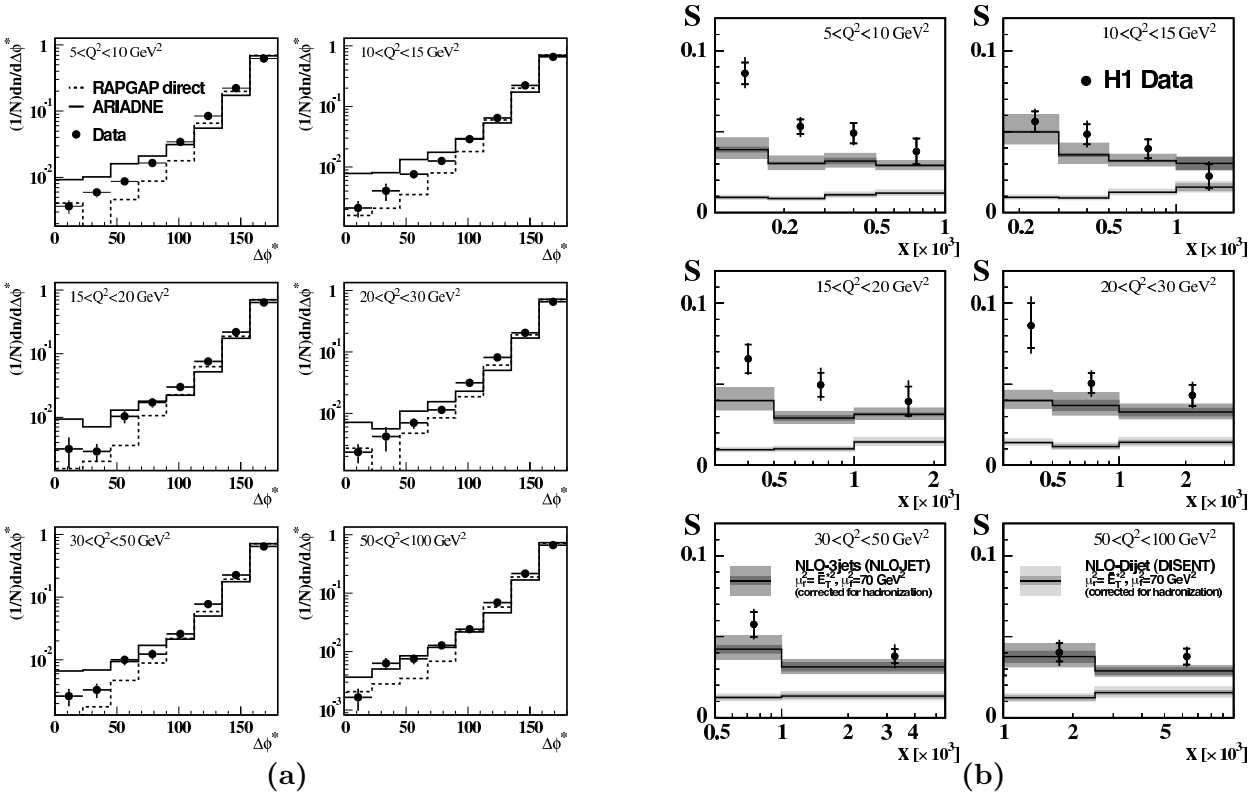

Figure 4: (a) Measured $\Delta\phi^*$ distribution in different regions of Q^2 (dots) [19]. For comparison, the predictions of RAPGAP and ARIADNE are also included. (b) Measured fraction S as a function of x in different Q^2 regions (dots) [19]. For comparison, the predictions of the fixed-order QCD calculations from DISENT and NLOJET are also included.

contain the lowest-order contribution to S, are several standard deviations below the data and show no dependence with x. On the other hand, the predictions of NLOJET, which incorporate NLO corrections to S, provide a good description of the data at large Q^2 and large x. However, they fail to describe the increase of the data towards low x values, especially at low Q^2. This shows the need to incorporate NLO corrections to the calculations.

Higher-order effects can be mimicked by the parton shower approach in Monte Carlo models. Figure 5a shows the comparison with the predictions of RAPGAP with direct only and resolved plus direct processes. A good description of the data is obtained at large Q^2 and large x. However, there is a failure to describe the strong rise of the data towards low x, especially at low Q^2, even when including a possible contribution from resolved virtual-photon processes, though the description in other regions is improved.

If the observed discrepancies are due to the influence of non-ordered parton emission, models based on the CDM or the CCFM evolution could provide a better description of the data. Figure 5b shows the data compared with ARIADNE and two predictions of CASCADE, which use different sets of unintegrated parton distributions. These sets differ in the way the small-k_T region is treated: in Jung2003 the full splitting function, i.e. including the non-singular term, is used in contrast to JS2001, for which only the singular term was considered. The predictions of ARIADNE give a good description of the data at low x and Q^2, but fail to describe the data at high Q^2. The predictions of CASCADE using JS2001 [15] lie significantly above the data in all x and Q^2 regions, whereas those using Jung2003 [20] are closer to the data. Therefore, the measurement of the fraction S is sensitive to and can be used to gain information on the

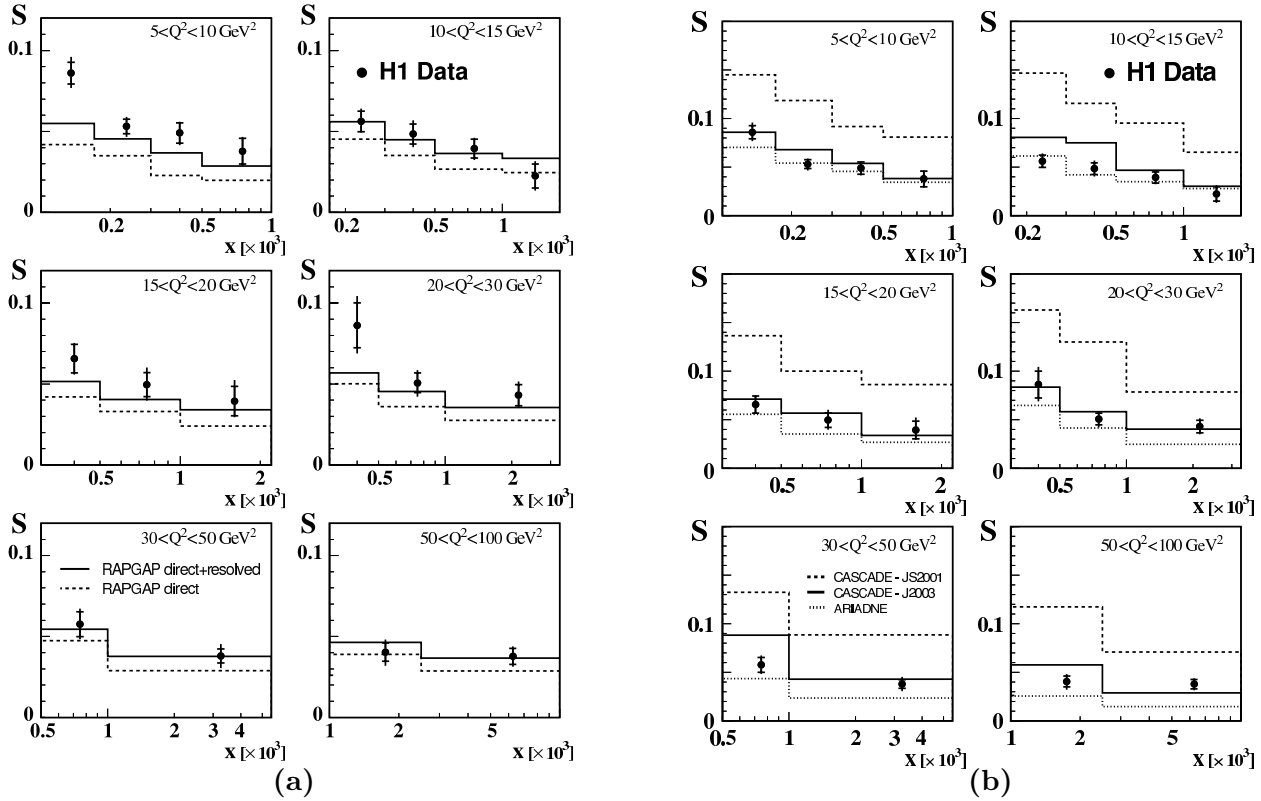

Figure 5: Measured fraction S as a function of x in different Q^2 regions (dots) [19]. For comparison, the predictions from (a) RAPGAP and (b) CASCADE and ARIADNE are also included.

unintegrated parton distributions.

3 Multi-jet production in NC DIS

Three-jet production in NC DIS provides a test of pQCD directly beyond LO since the since the lowest-order contribution is proportional to α_s^2. Three-jet events arise from additional gluon brehmstrahlung or splitting of a gluon into a $q\bar{q}$ pair (Fig. 6).

The dijet (three-jet) cross section has been measured [21] using the k_T cluster algorithm in the longitudinally invariant mode in the Breit frame for events with at least two (three) jets of $E_{T,\mathrm{B}}^{\mathrm{jet}} > 5$ GeV and $-1 < \eta_{\mathrm{LAB}}^{\mathrm{jet}} < 2.5$, and with dijet (three-jet) invariant masses in excess of 25 GeV; the kinematic region is defined by $10 < Q^2 < 5000$ GeV^2. Figure 7a shows the dijet and three-jet cross sections as a function of Q^2. The data are compared to the predictions of NLOJET up to $\mathcal{O}(\alpha_s^2)$ and $\mathcal{O}(\alpha_s^3)$, respectively, using $\mu_R^2 = Q^2 + (\bar{E}_{T,\mathrm{B}}^{\mathrm{jet}})^2$, where $\bar{E}_{T,\mathrm{B}}^{\mathrm{jet}}$ is the average jet transverse energy of the two (three) jets, and the factorisation scale $\mu_F = Q$. The CTEQ6 parametrisations of the proton PDFs have been used for the proton PDFs. The measured cross sections are well described by the predictions.

The Q^2 dependence of the ratio of the three-jet to the dijet cross section has been studied (see Fig. 7b). Many experimental and theoretical uncertainties cancel in the ratio and therefore this observable provides a more accurate test of color dynamics, especially at low Q^2 since the theoretical uncertainty of the ratio is of the same order as at higher Q^2. The calculations from NLOJET, using the five sets of the CTEQ4 "A-series" of proton PDFs, give a good description

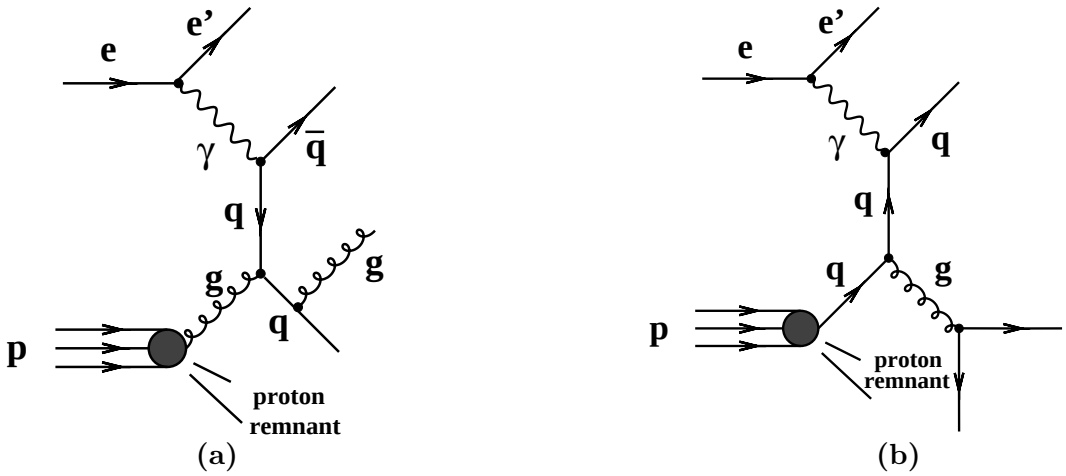

Figure 6: Examples of Feynman diagrams for three-jet production in NC DIS: (a) gluon brehmstrahlung from a quark and (b) gluon splitting into a $q\bar{q}$ pair.

of the data. The predictions for different values of α_s show the sensitivity of this observable to the value of $\alpha_s(M_Z)$ assumed in the calculations. A value of

$$\alpha_s(M_Z) = 0.1179 \pm 0.0013 \text{ (stat.)} \, ^{+0.0028}_{-0.0046} \text{ (exp.)} \, ^{+0.0061}_{-0.0047} \text{ (th.)}$$

has been extracted from the ratio, which is in good agreement with the world average, 0.1182 ± 0.0027 [22] and other determinations of α_s from HERA data.

4 Jet substructure and the dynamics of quarks and gluons

The internal structure of a jet depends mainly on the type of primary parton –quark or gluon– from which it originated and to a lesser extent on the particular hard scattering process. QCD predicts that at sufficiently high E_T^{jet}, where fragmentation effects become negligible, the jet structure is driven by gluon emission off the primary parton and is then calculable in pQCD. QCD also predicts that gluon jets are broader than quark jets due to the larger colour charge of the gluon. This prediction has been confirmed at LEP in measurements of the internal structure of jets [23].

The internal structure of jets has been studied by means of the jet shape. The integrated jet shape is defined as the fraction of the jet transverse energy that lies inside a cone in the $\eta - \varphi$ plane of radius r concentric with the jet axis, using only those particles belonging to the jet [24]:

$$\psi(r) = \frac{E_T(r)}{E_T^{\text{jet}}},$$

where $E_T(r)$ is the transverse energy within the given cone of radius r. The mean integrated jet shape, $\langle\psi(r)\rangle$, is defined as the averaged fraction of the jet transverse energy inside the cone of radius r:

$$\langle\psi(r)\rangle = \frac{1}{N_{\text{jets}}} \sum_{\text{jets}} \frac{E_T(r)}{E_T^{\text{jet}}},$$

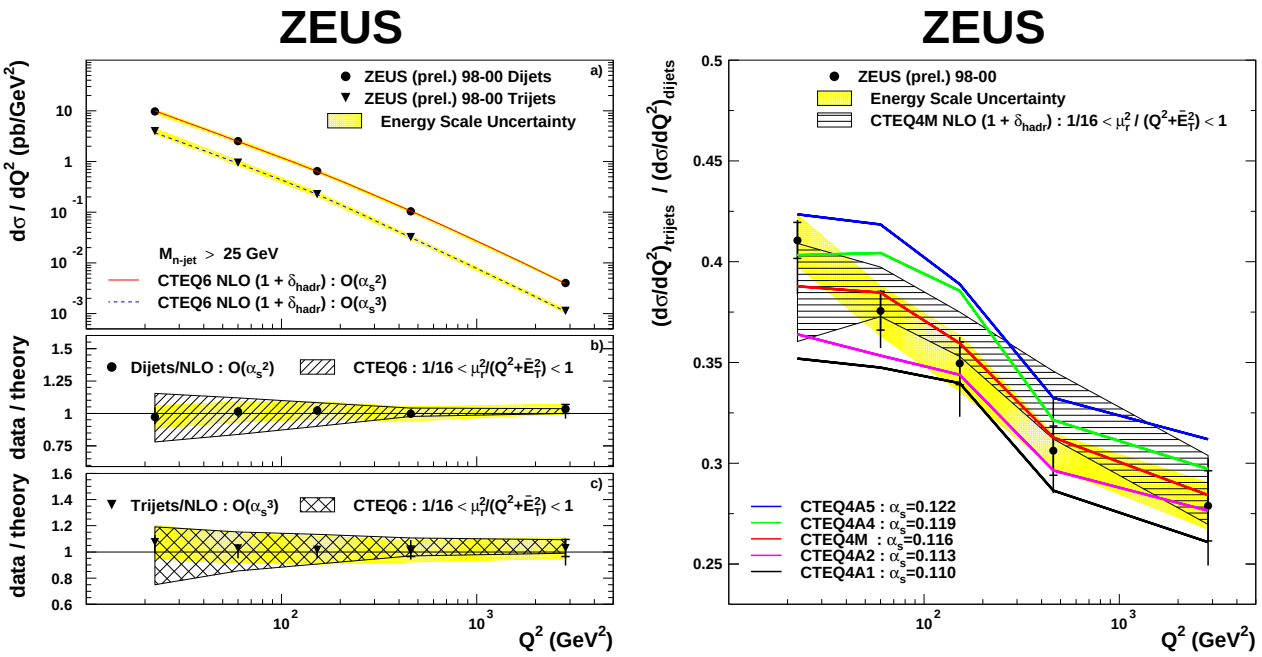

Figure 7: (a) Measured dijet and three-jet cross sections in NC DIS as a function of Q^2 (dots) [21]. (b) Measured ratio of the three-jet to the dijet cross section as a function of Q^2 (dots) [21]. For comparison, the predictions of NLOJET are also included in both figures.

where N_{jets} is the total number of jets in the sample.

The jets have been identified using the k_T cluster algorithm in the longitudinally inclusive mode and selected according to $E_T^{\text{jet}} > 17$ GeV and $-1 < \eta^{\text{jet}} < 2.5$. The kinematic region in the photoproduction sample is defined by $Q^2 < 1$ GeV^2 and $142 < W_{\gamma p} < 293$ GeV, where $W_{\gamma p}$ is the γp centre-of-mass energy, and in the NC DIS sample by $Q^2 > 125$ GeV^2.

4.1 Jet-shape measurements

The measured mean integrated jet shape as a function of r, $\langle\psi(r)\rangle$, for different regions in η^{jet} is shown in Fig. 8a for the photoproduction regime [25]. The jets broaden as η^{jet} increases. Leading-logarithm parton-shower predictions from PYTHIA [26] for resolved plus direct processes and for gluon- and quark-initiated jets are compared to the data in Fig. 8a. The measured $\langle\psi(r)\rangle$ is reasonably well described by the MC calculations of PYTHIA for resolved and direct processes for $-1 < \eta^{\text{jet}} < 1.5$, whereas for $1.5 < \eta^{\text{jet}} < 2.5$, the measured jets are slightly broader than the predictions. From the comparison with the predictions for gluon- and quark-initiated jets, it is seen that the measured jets are quark-like for $-1 < \eta^{\text{jet}} < 0$ and become increasingly more gluon-like as η^{jet} increases.

The measured $\langle\psi(r)\rangle$ for different regions of E_T^{jet} is shown in Fig. 8b for NC DIS events. The NLO QCD calculations of $\langle\psi(r)\rangle$, corrected for hadronisation and Z^0-exchange effects, are compared to the data in the figure. The NLO QCD calculations give a good description of $\langle\psi(r)\rangle$ for $r \geq 0.2$; the fractional differences between the measurements and the predictions are less than 0.2% for $r = 0.5$.

The quark and gluon content of the final state has been investigated in more detail by studying

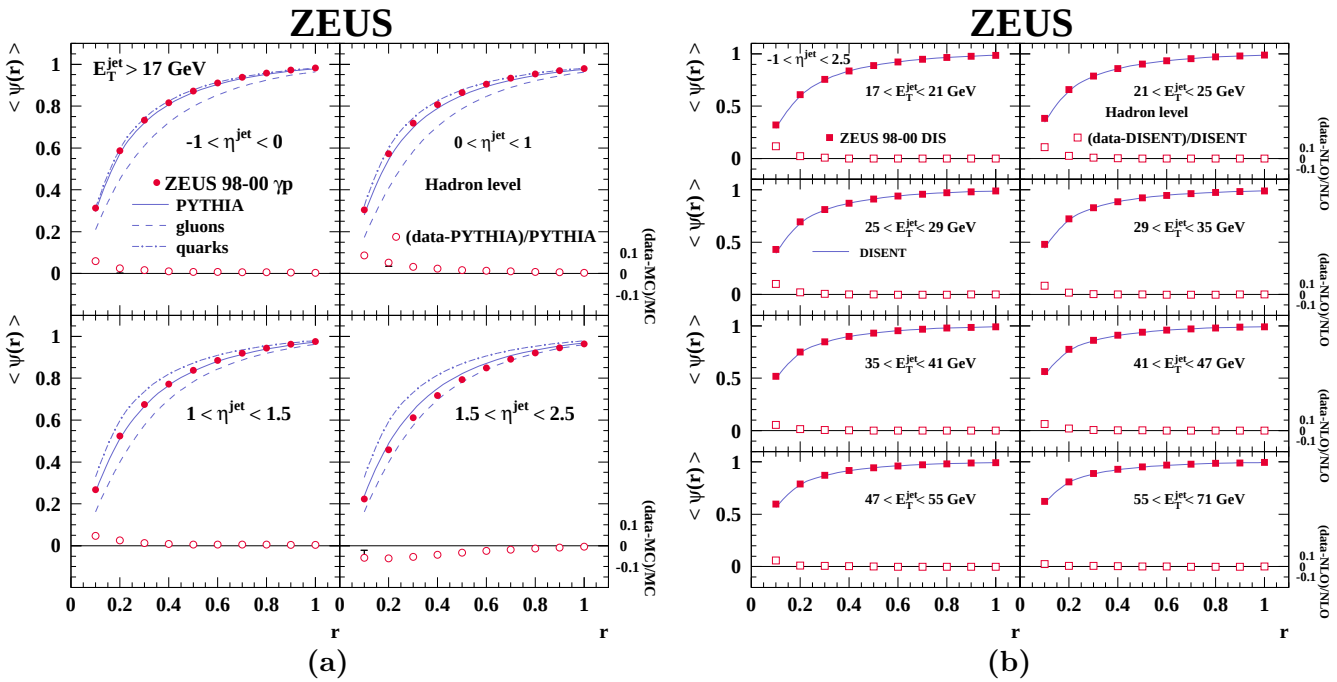

Figure 8: (a) Measured mean integrated jet shape as a function of r in different regions of $\eta^{\rm jet}$ in photoproduction (dots) [25]. (b) Measured mean integrated jet shape as a function of r in different $E_T^{\rm jet}$ regions in NC DIS (squares) [25]. For comparison, the predictions of (a) PYTHIA and (b) DISENT are also included.

the $\eta^{\rm jet}$ dependence of the mean integrated jet shape in photoproduction and NC DIS at a fixed value of $r = 0.5$ (see Fig. 9a). The jet shape at a fixed value of $r = 0.5$ decreases with increasing $\eta^{\rm jet}$ for photoproduction, whereas the jets in NC DIS show no dependence with $\eta^{\rm jet}$. The comparison of the data with the predictions for quark and gluon jets shows that the NC DIS jets are consistent with being dominated by quark jets, whereas the broadening of the jets in photoproduction is consistent with an increase of the fraction of gluon jets as $\eta^{\rm jet}$ increases. The dependence of the mean integrated jet shape for a fixed value of $r = 0.5$ as a function $E_T^{\rm jet}$ (see Fig.9b) in NC DIS shows that the jets become narrower as $E_T^{\rm jet}$ increases. The same is observed in photoproduction (not shown). The comparison of the data with the NLO calculations assuming different values of $\alpha_s(M_Z)$ shows the sensitivity of this observable to the value of $\alpha_s(M_Z)$. A value of α_s of

$$\alpha_s(M_Z) = 0.1176 \pm 0.0009\ (\text{stat.})\ ^{+0.0009}_{-0.0026}\ (\text{exp.})\ ^{+0.0091}_{-0.0072}\ (\text{th.})$$

was determined from this observable. This determination of α_s has experimental uncertainties as small as those based on previous measurements. However, the theoretical uncertainty is large and dominated by terms beyond NLO. Further theoretical work on higher-order contributions would allow an improved determination of α_s from the integrated jet shape in DIS.

4.2 Substructure dependence of jet cross sections

The predictions of the Monte Carlo for the jet shape reproduce well the data and show the expected differences for quark- and gluon-initiated jets. These differences are used to select samples enriched in quark and gluon jets to study in more detail the dynamics of the hard subprocesses. The predicted shapes of the distribution in $\psi(r = 0.3)$ for quark and gluon jets

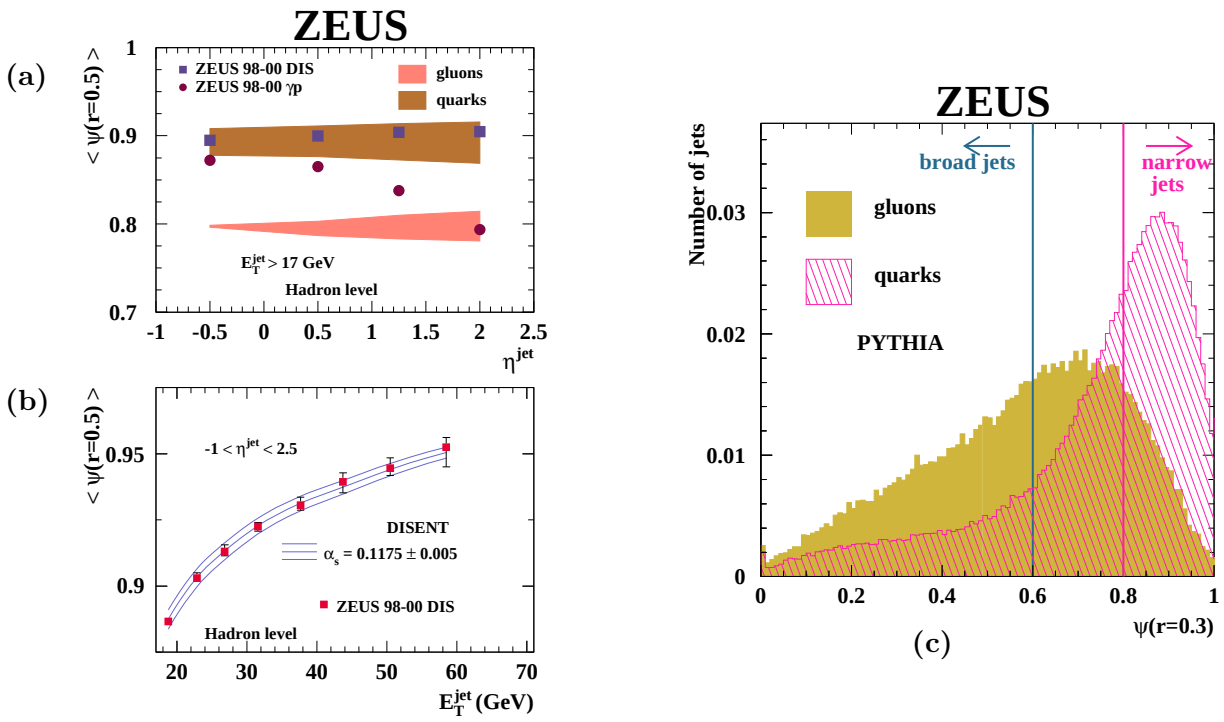

Figure 9: (a) Measured mean integrated jet shape at a fixed value of $r = 0.5$ as a function of $\eta^{\rm jet}$ in photoproduction (dots) and NC DIS (squares) [25]. For comparison, the Monte Carlo predictions for quark- and gluon-initiated jets are also included. (b) Measured mean integrated jet shape at a fixed value of $r = 0.5$ as a function of $E_T^{\rm jet}$ in NC DIS [25]. For comparison,the predictions of DISENT assuming three different values of α_s are also included. (c) Predicted integrated jet shape distributions from PYTHIA at $r = 0.3$ for quark- (hatched histogram) and gluon-initiated (shaded histogram) jets.

are different, as shown in Fig. 9c. A sample enriched in quark (or "narrow") jets was selected by requiring an integrated jet shape above 0.8 and a sample enriched in gluon (or "broad") jets was selected by requiring an integrated jet shape below 0.6. PYTHIA predicts a purity of 57% for gluons and 84% for quarks, and the efficiencies are 58% for gluons and 51% for quarks.

The differential inclusive-jet cross-section $d\sigma/d\eta^{\rm jet}$ for photoproduction is shown in Fig. 10a for samples of broad and narrow jets, separated according to the selection explained above. The measured cross sections exhibit different behaviours: the $\eta^{\rm jet}$ distribution for broad jets increases up to the highest $\eta^{\rm jet}$ value measured, whereas the distribution for narrow jets peaks at $\eta^{\rm jet} \approx 0.7$. Monte Carlo calculations using PYTHIA are compared to the measurements in Fig. 10a. The same selection method was applied to the jets of hadrons in the MC event samples and the calculations have been normalised to the total measured cross section of each sample. The MC predictions provide a good description of the shape of the narrow-jet distribution in the data. The shape of the broad-jet distribution in the data is reasonably well described by PYTHIA. From the calculation of PYTHIA, the sample of broad jets selected according to the jet shape is predicted to contain 15% of gg subprocesses in the final state and 50% of gq, and a contamination from processes with only quarks in the final state of 35%. There is a large contribution from gq final states in the broad-jet sample because the partonic cross section for the resolved subprocess $q_\gamma g_p \to qg$ is much larger than the cross section for the subprocesses $q\bar{q} \to gg$ plus $gg \to gg$. The sample of narrow jets contains 62% of qq subprocesses and

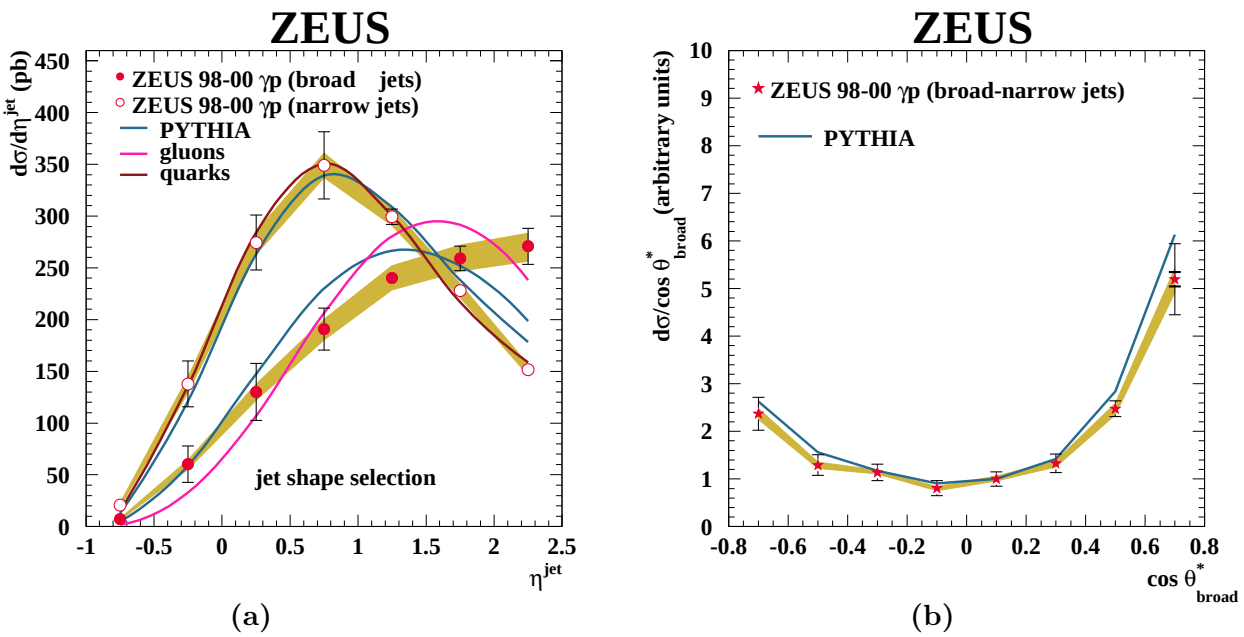

Figure 10: (a) Measured inclusive-jet cross section in photoproduction as a function of $\eta^{\rm jet}$ for samples of broad (dots) and narrow (open circles) jets [25]. (b) Measured dijet cross section in photoproduction as a function of $\cos\theta^*_{\rm broad}$ (stars) [25]. For comparison, the predictions of PYTHIA for jets selected in the same way as in the data and for quark- and gluon-initiated jets are included.

34% of qg, with a contamination of 4% from gg subprocesses. Figure 10a also shows the predictions of PYTHIA for jets of quarks and gluons separately. These predictions have been obtained without any selection and are normalised to the data cross sections. The calculation that includes only quark-initiated jets gives a good description of the narrow-jet cross section, whereas the calculation for gluon-initiated jets provides a reasonable description of the broad-jet cross section. This result supports the expectation that the broad (narrow)-jet sample is dominated by gluon (quark)-initiated jets.

The distribution in θ^*, where θ^* is the angle between the jet-jet axis and the beam direction in the dijet system, reflects the underlying parton dynamics and is sensitive to the spin of the exchanged particle. In the case of direct-photon interactions, the contributing subprocesses at LO QCD involve quark exchange and so $d\sigma/d|\cos\theta^*| \propto (1-|\cos\theta^*|)^{-1}$ as $|\cos\theta^*| \to 1$. In the case of resolved-photon interactions, the dominant subprocesses are those that involve gluon exchange and $d\sigma/d|\cos\theta^*| \propto (1-|\cos\theta^*|)^{-2}$ as $|\cos\theta^*| \to 1$. The study of the angular distribution for dijet events with tagged quark- and/or gluon-initiated jets in the final state, provides then a handle to investigate the underlying parton dynamics further.

The sample of photoproduced dijet events with one broad jet and one narrow jet was used to measure $d\sigma/d\cos\theta^*_{\rm broad}$, where $\theta^*_{\rm broad}$ refers to the scattering angle measured with respect to the broad jet. Figure 10b shows the measured dijet cross section as a function of $\cos\theta^*_{\rm broad}$. The measured and predicted cross sections were normalised to unity at $\cos\theta^*_{\rm broad} = 0.1$. The dijet angular distribution shows a different behaviour on the negative and positive sides; the measured cross section at $\cos\theta^*_{\rm broad} = 0.7$ is approximately twice as large as at $\cos\theta^*_{\rm broad} = -0.7$. The calculation from PYTHIA gives a good description of the shape of the measured $d\sigma/d\cos\theta^*_{\rm broad}$. The predictions of PYTHIA for the partonic content are: 52% of qg subprocesses, 4% of gg and 44% of qq. The observed asymmetry is adequately reproduced by the calculation

and is understood in terms of the dominant resolved subprocess $q_\gamma g_p \to qg$. The $\cos\theta^*_{\rm broad}$ distribution for this subprocess is asymmetric due to the different dominant diagrams in the regions $\cos\theta^*_{\rm broad} \to \pm 1$: t-channel gluon exchange ($\cos\theta^*_{\rm broad} \to +1$) and u-channel quark exchange ($\cos\theta^*_{\rm broad} \to -1$).

In conclusion, the hard subprocesses have been investigated separately in photoproduction for the first time using the internal structure of jets.

5 Conclusions

HERA has become a unique QCD-testing machine. At large scales considerable progress in understanding and reducing the experimental and theoretical uncertainties has led to very precise measurements of the fundamental parameter of the theory, the strong coupling constant α_s (see Fig. 11) as well as further insight into the dynamics of quarks and gluons. The use of observables based on the application of jet algorithms to the hadronic final state of deep inelastic scattering and of photon-proton interactions leads now to determinations that are as precise as those coming from more inclusive measurements, such as from τ decays. To obtain even better accuracy in the determination of α_s, further improvements in the QCD calculations are needed, e.g. next-to-next-to-leading-order corrections.

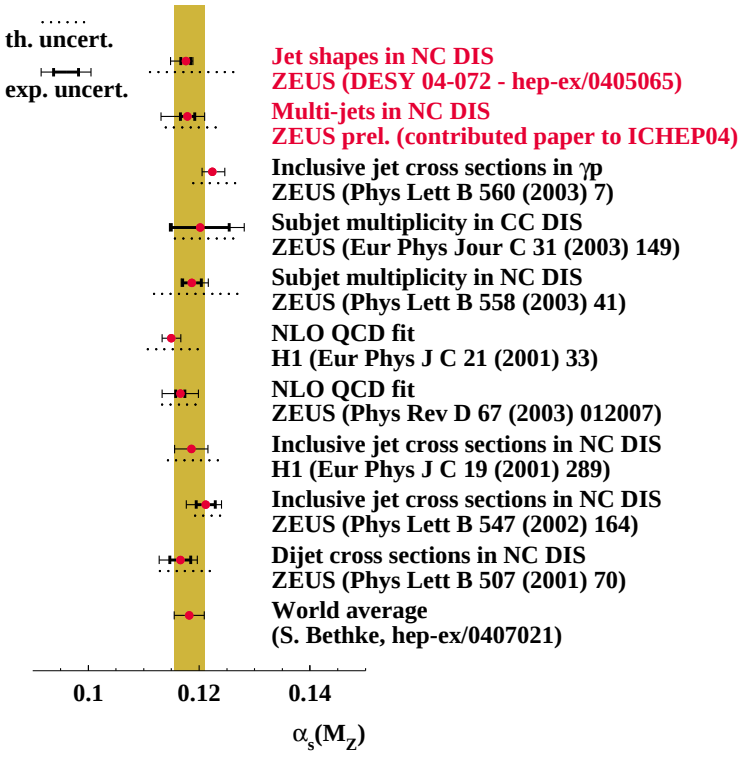

Figure 11: Summary of α_s determinations at HERA compared with the world average.

At low x considerable progress has also been obtained in understanding the mechanisms of parton emission, though the interplay between the DGLAP, BFKL and CCFM evolution schemes has still to be fully worked out. Further progress in this respect needs both more experimental and more theoretical work.

Acknowledgments

I would like to thank the organisers for providing a warm atmosphere conducive to many physics discussions and a well organised conference. Special thanks to my colleagues from H1 and ZEUS for their help in preparing this report.

References

[1] ZEUS Coll., M. Derrick et al., *Phys. Lett.* **B** 316 (1993) 412;
ZEUS Coll., M. Derrick et al., *Z. Phys.* **C** 65 (1995) 379;
ZEUS Coll., M. Derrick et al., *Phys. Lett.* **B** 345 (1995) 576;
ZEUS Coll., M. Derrick et al., *Z. Phys.* **C** 69 (1996) 607;
ZEUS Coll., M. Derrick et al., *Z. Phys.* **C** 72 (1996) 399;
ZEUS Coll., J. Breitweg et al., *Phys. Lett.* **B** 407 (1997) 432;
ZEUS Coll., J. Breitweg et al., *Eur. Phys. Jour.* **C** 7 (1999) 609;
ZEUS Coll., J. Breitweg et al., *Eur. Phys. Jour.* **C** 11 (1999) 27;
ZEUS Coll., J. Breitweg et al., *Phys. Lett.* **B** 487 (2000) 53;
ZEUS Coll., J.Breitweg et al., *Eur. Phys. Jour.* **C** 12 (2000) 411; Erratum in *Eur. Phys. Jour.* **C** 27 (2003) 305;
ZEUS Coll., S. Chekanov et al., *Eur. Phys. Jour.* **C** 21 (2001) 443;
ZEUS Coll., S. Chekanov et al., *Phys. Lett.* **B** 539 (2002) 197; Erratum in *Phys. Lett.* **B** 552 (2003) 308
ZEUS Coll., S. Chekanov et al., *Phys. Rev.* **D** 67 (2003) 012007;
ZEUS Coll., S. Chekanov et al., *Eur. Phys. Jour.* **C** 28 (2003) 175;
ZEUS Coll., S. Chekanov et al., *Eur. Phys. Jour.* **C** 32 (2003) 1;
ZEUS Coll., S. Chekanov et al., *Phys. Rev.* **D** 70 (2004) 052001.

[2] H1 Coll., I. Abt et al., *Nucl. Phys.* **B** 407 (1993) 515;
H1 Coll., I. Abt et al., *Phys. Lett.* **B** 321 (1994) 161;
H1 Coll., T. Ahmed et al., *Nucl. Phys.* **B** 439 (1995) 471;
H1 Coll., S. Aid et al., *Phys. Lett.* **B** 354 (1995) 494;
H1 Coll., S. Aid et al., *Nucl. Phys.* **B** 449 (1995) 3;
H1 Coll., S. Aid et al., *Nucl. Phys.* **B** 470 (1996) 3;
H1 Coll., C. Adloff et al., *Phys. Lett.* **B** 393 (1997) 452;
H1 Coll., C. Adloff et al., *Nucl. Phys.* **B** 497 (1997) 3;
H1 Coll., C. Adloff et al., *Eur. Phys. Jour.* **C** 13 (2000) 609;
H1 Coll., C. Adloff et al., *Eur. Phys. Jour.* **C** 21 (2001) 33;
H1 Coll., C. Adloff et al., *Eur. Phys. Jour.* **C** 19 (2001) 269;
H1 Coll., C. Adloff et al., *Phys. Lett.* **B** 520 (2001) 183;
H1 Coll., C. Adloff et al., *Eur. Phys. Jour.* **C** 30 (2003) 1;
H1 Coll., A. Aktas et al., DESY 04-083 (hep-ex/0406029).

[3] BCDMS Coll., A.C. Benvenuti et al., *Phys. Lett.* **B** 223 (1989) 485;
BCDMS Coll., A.C. Benvenuti et al., *Phys. Lett.* **B** 237 (1990) 592;
L.W. Whitlow et al., *Phys. Lett.* **B** 282 (1992) 475;
E665 Coll., M.R. Adams et al., *Phys. Rev.* **D** 54 (1996) 3006;
NMC Coll., M. Arneodo et al., *Nucl. Phys.* **B** 483 (1997) 3;

NMC Coll., M. Arneodo et al., *Nucl. Phys.* **B** 487 (1997) 3;
CCFR Coll., W.G. Seligman et al., *Phys. Rev. Lett.* 79 (1997) 1213;
FNAL E866/NuSea Coll., E.A. Hawker et al., *Phys. Rev. Lett.* 80 (1998) 3715.

[4] V.N. Gribov and L.N. Lipatov, *Sov. J. Nucl. Phys.* 15 (1972) 438;
L.N. Lipatov, *Sov. J. Nucl. Phys.* 20 (1975) 94;
G. Altarelli and G. Parisi, *Nucl. Phys.* **B** 126 (1977) 298;
Yu.L. Dokshitzer, *Sov. Phys. JETP* 46 (1977) 641.

[5] ZEUS Coll., M. Derrick et al., *Phys. Lett.* **B** 306 (1993) 158;
ZEUS Coll., M. Derrick et al., *Z. Phys.* **C** 67 (1995) 81;
ZEUS Coll., M. Derrick et al., *Phys. Lett.* **B** 363 (1995) 201;
ZEUS Coll., J. Breitweg et al., *Eur. Phys. Jour.* **C** 6 (1999) 239;
ZEUS Coll., J. Breitweg et al., *Eur. Phys. Jour.* **C** 8 (1999) 367;
ZEUS Coll., J. Breitweg et al., *Phys. Lett.* **B** 474 (2000) 223;
ZEUS Coll., J. Breitweg et al., *Phys. Lett.* **B** 507 (2001) 70;
ZEUS Coll., S. Chekanov et al., *Eur. Phys. Jour.* **C** 23 (2002) 13;
ZEUS Coll., S. Chekanov et al., *Phys. Lett.* **B** 547 (2002) 164;
ZEUS Coll., S. Chekanov et al., *Phys. Lett.* **B** 551 (2003) 3;
ZEUS Coll., S. Chekanov et al., *Phys. Lett.* **B** 558 (2003) 41;
ZEUS Coll., S. Chekanov et al., *Eur. Phys. Jour.* **C** 31 (2003) 149;
ZEUS Coll., S. Chekanov et al., *Eur. Phys. Jour.* **C** 35 (2004) 487.

[6] H1 Coll., I. Abt et al., *Z. Phys.* **C** 61 (1994) 59;
H1 Coll., T. Ahmed et al., *Phys. Lett.* **B** 346 (1995) 415;
H1 Coll., S. Aid et al., *Phys. Lett.* **B** 356 (1995) 118;
H1 Coll., C. Adloff et al., *Phys. Lett.* **B** 415 (1997) 418;
H1 Coll., C. Adloff et al., *Eur. Phys. Jour.* **C** 5 (1998) 625;
H1 Coll., C. Adloff et al., *Eur. Phys. Jour.* **C** 6 (1999) 575;
H1 Coll., C. Adloff et al., *Nucl. Phys.* **B** 538 (1999) 3;
H1 Coll., C. Adloff et al., *Nucl. Phys.* **B** 545 (1999) 3;
H1 Coll., C. Adloff et al., *Eur. Phys. Jour.* **C** 13 (2000) 397;
H1 Coll., C. Adloff et al., *Eur. Phys. Jour.* **C** 13 (2000) 415;
H1 Coll., C. Adloff et al., *Eur. Phys. Jour.* **C** 19 (2001) 289;
H1 Coll., C. Adloff et al., *Eur. Phys. Jour.* **C** 19 (2001) 429;
H1 Coll., C. Adloff et al., *Phys. Lett.* **B** 515 (2001) 17;
H1 Coll., C. Adloff et al., *Eur. Phys. Jour.* **C** 24 (2002) 33;
H1 Coll., C. Adloff et al., *Phys. Lett.* **B** 542 (2002) 193.

[7] ZEUS Coll., M. Derrick et al., *Phys. Lett.* **B** 297 (1992) 404;
ZEUS Coll., M. Derrick et al., *Phys. Lett.* **B** 322 (1994) 287;
ZEUS Coll., M. Derrick et al., *Phys. Lett.* **B** 342 (1995) 417;
ZEUS Coll., M. Derrick et al., *Phys. Lett.* **B** 348 (1995) 665;
ZEUS Coll., M. Derrick et al., *Phys. Lett.* **B** 384 (1996) 401;
ZEUS Coll., J. Breitweg et al., *Eur. Phys. Jour.* **C** 2 (1998) 61;
ZEUS Coll., J. Breitweg et al., *Eur. Phys. Jour.* **C** 1 (1998) 109;
ZEUS Coll., J. Breitweg et al., *Eur. Phys. Jour.* **C** 4 (1998) 591;
ZEUS Coll., J. Breitweg et al., *Phys. Lett.* **B** 443 (1998) 394;
ZEUS Coll., J. Breitweg et al., *Eur. Phys. Jour.* **C** 11 (1999) 35;

ZEUS Coll., J. Breitweg et al., *Phys. Lett.* **B** 479 (2000) 37;
ZEUS Coll., S. Chekanov et al., *Phys. Lett.* **B** 531 (2002) 9;
ZEUS Coll., S. Chekanov et al., *Eur. Phys. Jour.* **C** 23 (2002) 615;
ZEUS Coll., S. Chekanov et al., *Phys. Lett.* **B** 560 (2003) 7.

[8] H1 Coll., T. Ahmed et al., *Phys. Lett.* **B** 297 (1992) 205;
H1 Coll., I. Abt et al., *Phys. Lett.* **B** 314 (1993) 436;
H1 Coll., T. Ahmed et al., *Nucl. Phys.* **B** 445 (1995) 195;
H1 Coll., S. Aid et al., *Z. Phys.* **C** 70 (1996) 17;
H1 Coll., C. Adloff et al., *Eur. Phys. Jour.* **C** 1 (1998) 97;
H1 Coll., C. Adloff et al., *Phys. Lett.* **B** 483 (2000) 36;
H1 Coll., C. Adloff et al., *Eur. Phys. Jour.* **C** 25 (2002) 13;
H1 Coll., C. Adloff et al., *Eur. Phys. Jour.* **C** 29 (2003) 497.

[9] V.S. Fadin, E.A. Kuraev and L.N. Lipatov, *Sov. Phys. JETP* 44 (1976) 443;
V.S. Fadin, E.A. Kuraev and L.N. Lipatov, *Sov. Phys. JETP* 45 (1977) 199;
Y. Balitsky and L.N. Lipatov, *Sov. J. Nucl. Phys.* 28 (1978) 822.

[10] M. Ciafaloni, *Nucl. Phys.* **B** 296 (1988) 49;
S. Catani, F. Fiorani and G. Marchesini, *Phys. Lett.* **B** 234 (1990) 339;
S. Catani, F. Fiorani and G. Marchesini, *Nucl. Phys.* **B** 336 (1990) 18;
G. Marchesini, *Nucl. Phys.* **B** 445 (1995) 49.

[11] H. Jung, L. Jönsson and H. Küster, *Eur. Phys. Jour.* **C** 9 (1999) 383.

[12] S. Catani and M.H. Seymour, *Nucl. Phys.* **B** 485 (1997) 291. Erratum in *Nucl. Phys.* **B** 510 (1998) 503.

[13] Z. Nagy and Z. Trocsanyi, *Phys. Rev. Lett.* 87 (2001) 082001.

[14] H. Jung, *Comp. Phys. Comm.* 86 (1995) 147.

[15] H. Jung and G.P. Salam, *Eur. Phys. Jour.* **C** 19 (2001) 351;
H. Jung, *Comp. Phys. Comm.* 143 (2002) 100.

[16] L. Lönnblad, *Comp. Phys. Comm.* 71 (1992) 15;
L. Lönnblad, *Z. Phys.* **C** 65 (1995) 285.

[17] H1 Coll., Contributed paper N 5-0172 to the 32nd International Conference on High Energy Physics, August 16-22,2004, Beijing.

[18] A.H. Mueller and H. Navelet, *Nucl. Phys.* **B** 282 (1987) 727.

[19] H1 Coll., A. Aktas et al., *Eur. Phys. J.* **C33**, 477 (2004).

[20] M. Hansson and H. Jung, Preprint hep-ph/0309009, 2003.

[21] ZEUS Coll., Contributed paper N 5-0294 to the 32nd International Conference on High Energy Physics, August 16-22,2004, Beijing.

[22] S. Bethke, Preprint hep-ex/0407021, 2004.

[23] OPAL Coll., G. Alexander et al., *Phys. Lett.* **B** 265 (1991) 462;
OPAL Coll., P.D. Acton et al., *Z. Phys.* **C** 58 (1993) 387;
OPAL Coll., R. Akers et al., *Z. Phys.* **C** 68 (1995) 179;
OPAL Coll., G. Alexander et al., *Z. Phys.* **C** 69 (1996) 543;
OPAL Coll., G. Abbiendi et al., *Eur. Phys. Jour.* **C** 11 (1999) 217;
OPAL Coll., G. Abbiendi et al., *Phys. Rev.* **D** 69 (2004) 032002;
DELPHI Coll., P. Abreu et al., *Z. Phys.* **C** 70 (1996) 179;
DELPHI Coll., P. Abreu et al., *Eur. Phys. Jour.* **C** 13 (2000) 573;
ALEPH Coll., D. Buskulic et al., *Phys. Lett.* **B** 384 (1996) 353;
ALEPH Coll., R. Barate et al., *Eur. Phys. Jour.* **C** 17 (2000) 1.

[24] S.D. Ellis, Z. Kunszt and D.E. Soper, *Phys. Rev. Lett.* 69 (1992) 3615.

[25] ZEUS Coll., S. Chekanov et al., DESY 04-072 and hep-ex/0405065.

[26] T. Sjöstrand, *Comp. Phys. Comm.* 82 (1994) 74;
T. Sjöstrand et al., *Comp. Phys. Comm.* 135 (2001) 238.